Lifted Flame Structure of Coannular Jet Flames in a Triple Port Burner

by

Kazuhiro YAMAMOTO, Shinya KATO, Yusuke ISOBE, Naoki HAYASHI, Hiroshi YAMASHITA
Department of Mechanical Science and Engineering
Nagoya University, Furo-cho, Chikusa-ku, Nagoya, Aichi 464-8603, JAPAN

ABSTRACT

In this study, we investigated the combustion field in a triple port burner. The coannular burner consists of three concentric tubes, where air flows in both inner (central) and outer tubes, and fuel flows in the annulus between these air tubes. In order to investigate the combustion characteristics in the triple port burner, the liftoff height and concentrations of soot and NOx were experimentally examined. A numerical simulation was also conducted to discuss the flame structure in detail. Since two non-premixed flames are formed in the boundaries of fuel and air, there are four flame configurations, consisting of attached flames, inner attached/outer lifted flames, inner lifted/outer attached flames, and twin lifted flames. By increasing the external air flow velocity, unique flame behaviors are observed, including (1) inner flame re-attachment and (2) flip-flop between inner and outer flames. When the flame is lifted, the maximum soot concentration and NOx emission are decreased. Based on the flame index, the attached flame is mainly a diffusion flame. When the inner or outer flame is lifted, the so-called triple flame structure is observed. Interestingly, in the case of twin lifted flames, two rich premixed flames are merged each other.

Introduction

Due to the regulations of pollutants, we need to reduce emissions of nitrogen oxides (NOx) and soot particles in combustion. It is well known that NOx are pollutants to produce acid rain and photo-chemical smog. On the other hand, soot particles can penetrate into lung tissue and lead to serious pulmonary edema and cancer [1,2].

As for the NOx reduction, fundamental studies have been made. Since prompt NO is not very sensitive to temperature, thermal NO formation should be reduced when we need to improve high NO levels that occur in practical systems [3]. In general, different from premixed combustion under which fuel and oxidizer are thoroughly mixed, it is difficult to control the flame temperature in non-premixed combustion, because the flame is expectedly formed at a stoichiometric region. So far, various methods have been proposed to reduce NOx emissions. For example, by using swirl flow, rapid mixing between fuel and air has been examined [4-6]. Flue gas recirculation is also well-know method to control NOx in industrial burners [7]. The large reduction of NOx has been reported by the effect of dilution with burned gas, combined with the flame stretch [8]. Zhao et al. [9] have studied NOx emission in diffusion flame with steam addition.

Here, we have focused on a lifted flame [10-16]. When the flame is stabilized with a large liftoff height, the injected fuel is partially premixed with surrounding air, and this causes a reduction in the flame temperature, resulting in low NOx emission. As for the liftoff characteristics, it is important to consider the local flame structure involving lean and rich premixed flames and a diffusion flame, which is called a triple flame. Recent simulation has suggested that there are large diffusion flame islands at the base of a turbulent jet lifted flame, which would provide heat-release and radicals [17,18]. However, it is expected that a large number of flamelets exist in the turbulent case, the flame and flow interactions are too complex [19-22].

In the present study, we focus on a triple port burner [23,24]. The burner configuration is quite similar to a coannular burner for inverse diffusion flames [25-27]. The burner has three concentric tubes, where air

flows in both inner (central) and outer tubes and fuel flows in the annulus between air tubes (see **Fig. 1**). Since there are two boundaries between fuel and air, two non-premixed flames are formed. Measurements of NOx and soot concentrations are conducted, discussed with the variations of liftoff characteristics. Additionally, we simulate the combustion field to observe the flame behavior and visualize the flame structure in the triple port burner.

Experimental setup

Triple port burner

Figure 1 shows a schematic of the triple port burner. Since the fuel is supplied between two air flows, it is expected that the mixing between fuel and air is promoted in comparison with a co-axial diffusion burner [23,24]. The internal air flow nozzle has an inner diameter of 10 mm (rim thickness of 1 mm), the fuel flow nozzle has an inner diameter of 14 mm, the external air flow nozzle has an inner diameter of 27 mm. Methane was used for fuel. The velocities of internal and external air flows, U_{1A} and U_{3A}, were varied, while the fuel flow velocity was fixed at U_{2F} = 0.6 m/s. As for the coordinate system, *r* and *z* represent the radial and axial distances from the center of the burner exit, respectively.

Fig.1

Measurements

The soot concentration was measured using LII. For the light source, the second harmonic (wavelength of λ = 532 nm) of a Nd:YAG laser (PRO-R10, manufactured by Spectra Physics) was used. A laser sheet was passed through the flame to heat the soot particles up to incandescence temperature. The LII signal from soot was measured with a gated image-intensified CCD camera (Hamamatsu Photonics C8484). The CCD camera has a resolution of 1024 × 1024 pixels, and the image size was 37 × 37 mm. In this

measurement, the laser beam thickness is about 400 μm. A band-pass filter (FWHM = 10 nm) with the central wavelength at 400 nm was installed in front of ICCD camera [28]. The image intensifier gate width was set at 50 ns in order to eliminate light emitted from the flame and background. Although, in our preliminary experiments, it has been confirmed that LII signal is simply proportional to soot volume fraction [29], any calibrations were not conducted for LII signals. The soot measurement was performed in the range of $-18.5 \leq r \leq 18.5$ mm and $31.5 \leq z \leq 98.5$ mm.

On the other hand, NOx concentration in burned gas was measured using a NOx analyzer (ECL-88A; Anatec Yanaco Corp., Japan). A gas sampling was conducted to collect the burned gas [30]. The sampling line was heated over 100 °C to avoid H_2O condensation. A preprocessing unit (CFP-8000; Shimazu Corp., Japan) was also used to remove water and soot particles.

Numerical analysis

Figure 2 shows an analytical model and the coordinate system. Two-dimensional axial symmetry is assumed. As explained before, the triple port burner is constructed in such a way that air (nozzle 1), fuel (nozzle 2), and then air (nozzle 3) again are injected, in that order, into the same axial stream. We set the another air inlet next to nozzle 3 to form the surrounding air with nominal velocity. Fuel is methane. The computational domain is 16.8 mm in the radial direction and –1 to 200 mm in the axial direction. Referring to the experiments, the inner radius of the inner air flow nozzle is 5 mm, that of the fuel flow nozzle is 7 mm, and that of the outer air flow nozzle is 13.5 mm. The thickness of each rim is 1 mm. As for the boundary conditions, a symmetric condition was applied at the central axis, and a free outflow condition was applied at the outlet. For the numerical stability, a non-slip wall condition was applied at the opposite sidewall. Although this condition may be different from the real situation, a good agreement between velocity fields obtained by simulation and PIV

Fig.2

measurements was confirmed in our preliminary experiments. At the inlet, the inflow condition was set to be the same as those in experiments.

The model, assumptions, and numerical techniques are found in our references [9,31,32]. The conservation equations of mass, momentum, energy, and species were solved by a finite volume method. For these time-dependent conservation equations, the time advance was performed to observe the flame behavior. As for the reaction scheme, Smooke's skeletal methane-air reaction mechanism, consisting of 16 chemical species and 25 elementary reactions, was used [33].

Results and discussion

Appearance of flame

Since there are two boundaries of fuel and air, two (inner and outer) flames are formed in the triple port burner. **Figure 3** shows photographs of flames. Four flame configurations are observed; namely, attached flames (**Fig. 3a**) in which inner and outer flames are attached to the burner rims between fuel and air flows, inner attached/outer lifted flames (**Fig. 3b**) in which only the outer flame is lifted, inner lifted/outer attached flames (**Fig. 3c**) in which only the inner flame is lifted, and twin lifted flames (**Fig. 3d**) in which both inner and outer flames are lifted.

Fig.3

Figure 4 shows a phase diagram to classify the flame structure. In this figure, I and O represent inner and outer flames. The subscripts A, L, and B represent the three flame configurations of attached, lifted, and blow off, respectively. The boundary of each flame configuration is determined by the following procedure; the internal air flow velocity is firstly set, and then the flame behavior is observed by increasing the external air flow velocity from zero to 1.2 m/s. For example, at U_{1A} = 0.3 m/s, attached flames are formed when U_{3A} is

Fig.4

set to be zero. As U_{3A} is increased, inner attached/outer lifted flames are formed. When U_{3A} is further increased, the outer lifted flame blows off. However, when U_{1A} is in the range of 0.49 to 0.65 m/s, another transition is observed. Firstly, both flames are attached at U_{3A} = 0 m/s, and then, only the inner flame is lifted as U_{3A} is increased. When U_{3A} exceeded 0.65 m/s, inner attached/outer lifted flames are formed. That is, the flip-flop behavior between inner and outer flames occurs, which has not been reported elsewhere. On the other hand, when U_{1A} exceeds 0.65 m/s, twin lifted flames are observed between the transition of inner lifted/outer attached flames and inner attached/outer lifted flames.

Liftoff height

Figure 5 shows the variations of liftoff height (L_f) with external air flow velocity. Liftoff heights for inner and outer flames were examined. The internal air flow velocity is U_{1A} = 0.4, 0.6, 0.8 m/s, respectively. In the case of U_{1A} = 0.4 m/s, both inner and outer flames are initially attached to the burner rims between fuel and air flows, and the outer flame is then lifted at U_{3A} = 0.49 m/s. When U_{3A} is raised further, the liftoff height of the outer flame became larger. In the case of U_{1A} = 0.6 m/s, both inner and outer flames are initially attached to the burner rims, and the inner flame is lifted at U_{3A} = 0.25 m/s. The inner lifted flame is then attached to the burner rim again at U_{3A} = 0.65 m/s. Simultaneously, the outer flame is lifted, forming inner attached/outer lifted flames. When U_{3A} is raised further, the liftoff height of the outer flame became larger. In the case of U_{1A} = 0.8 m/s, the inner flame is already lifted even though U_{3A} is set to be zero. In the range of $0.65 < U_{3A} < 0.9$ m/s, the outer flame is also lifted and twin lifted flames are observed. As shown in this figure, the liftoff height of twin lifted flames is much larger than that of the inner or outer flame when they are lifted alone. At U_{3A}= 0.9 m/s, inner attached/outer lifted flames are formed. It seems unclear that the inner flame is re-attached to the burner rim when the external air flow velocity is increased, which will be discussed later.

Fig.5

Measurements of soot and NOx

Next, measurements of soot and NOx concentrations were conducted. **Figure 6** shows the variations of maximum LII signal with the external air flow velocity, U_{3A}. The internal air flow velocity, U_{1A}, is 0.4, 0.6, 0.8 m/s. In these figures, the liftoff heights of inner and outer flames are also shown. In each LII image, the maximum value in the luminous flame was obtained, and the averaged value using 100 images was calculated and plotted. Since the LII signal is proportional to the soot volume fraction, it is possible to discuss the soot concentration at different flow conditions [29]. In the case of U_{1A} = 0.4 m/s, the maximum soot concentration rapidly decreases when the outer flame is lifted. In the case of U_{1A} = 0.6 m/s, the maximum soot concentration is also reduced when the inner flame is lifted. On the other hand, in the case of U_{1A} = 0.8 m/s, the soot concentration is almost zero, because the inner flame or outer flame is always lifted.

Fig.6

Figure 7 shows NOx emission index with changing the external air flow velocity. The flow conditions are the same in **Fig. 6**. In **Fig. 7c**, NOx emission index was not measured above U_{3A}= 0.65 m/s, because twin lifted flames were attached to the quartz tube, which was used to collect burned gas in downstream. It is found that the NOx emission index is decreased only when the outer flame is lifted. Clearly shown in **Fig. 3**, this may be simply because outer flame is much bigger. Therefore, the maximum soot concentration and NOx emission are decreased when the flame is lifted, which could be explained with the partially premixing effect [30]. To study further, the numerical simulation was conducted.

Fig.7

Simulation results

To investigate the flame structure in detail, we simulated the combustion field in the triple port burner. According to the experiments, the external air flow velocity is increased, keeping the constant velocities of fuel and internal air flows. **Figure 8** shows the distributions of temperature, mass fractions of methane and oxygen, and heat release rate. The internal air flow velocity is U_{1A} = 0.7 m/s and the fuel flow velocity is U_{2F} = 0.6 m/s. In this case,

Fig.8

the external air flow velocity is U_{3A} = 0.1 m/s. Similar to the experiment in **Fig. 3a**, both flames are attached.

Then, only external air flow velocity is increased. **Figure 9** shows the distributions of heat release rate at U_{3A} = 0.1, 0.4, 0.8 and 1.1 m/s. As shown in this figure, when U_{3A} is increased to 0.4 m/s, only the inner flame is lifted. Since the minimum quenching distance for methane/air mixture is 2 mm, which is larger than the rim thickness of 1 mm, the lifted mechanism is explained based on a balance between the entrained-stream velocity at the flame base and the local burning velocity [11]. Then, at U_{3A} = 0.8 m/s, the outer flame is also lifted, and twin lifted flames are formed. When U_{3A} is raised further, the inner lifted flame is re-attached. Thus, these flame behaviors well correspond to experiments.

Fig.9

To discuss the flame structure, we examine the flame index, which is given by the following equation [32]:

$$G_{FO} = \mathrm{grad}Y_F \cdot \mathrm{grad}Y_O \quad (Q > 0.01 \times Q_{\max})$$

where G_{FO} is positive for a premixed flame and negative for a diffusion flame, Q is the heat release rate, and $Q_{\max}$ is the maximum heat release rate. **Figure 10** shows the distributions of flame index obtained at the conditions in **Fig. 9.** When both inner and outer flames are attached, two diffusion flames are mainly formed, except that the premixed flame is formed near the burner rim. When U_{1A} is 0.4 m/s, a so-called triple flame, consisting of a lean premixed flame, a diffusion flame, and a rich premixed flame, is observed for the inner lifted flame. When U_{1A} is further raised to 0.8 m/s, twin lifted flames are formed, where two triple flames are observed. Interestingly, two rich premixed flames are merged each other.

Fig.10

When a flame is lifted, fuel and air are partially mixed. Since the lifted flame edge has a triple flame structure, the maximum temperature at the edge is not changed much (see Fig. 11). However, the diffusion flame length of high temperature is largely reduced, mainly caused by the air entrainment [12]. Also, the temperature decrease of rich premixed flames is observed. Consequently, the low NOx emission is achieved.

At the same time, the soot formation is reduced by the decrease of flame length, resulting in the lower soot concentration in the luminous flame zone.

As mentioned before, when U_{3A} is further raised to 1.1 m/s, the inner lifted flame is re-attached. To investigate this flame behavior, the time-variations of temperature and heat release rate are examined at U_{3A} = 1.0 to 1.1 m/s. These results are shown in **Figs. 11 and 12**, obtained at t = 40, 120, 240, 300, and 400 ms. For further discussion, the temperatures of inner and outer flames at the leading flame edge are shown in **Fig. 11**. It should be noted that the motion of the inner flame begins when the liftoff height of the outer flame is larger than that of the inner flame. Clearly, the inner flame is moving against the inflow direction. It is well known that there are two factors to determine the liftoff height. One is the burning velocity of the lifted flame. The other is the inflow velocity toward the base of the lifted flame. Based on the simulation results, the temperature at the inner flame edge is almost constant even when the external air flow velocity is increased. Also, the heat release rate of flame edge in **Fig. 12** is not changed largely.

Thus, we focus on the inflow velocity near the flame edge at the location where the temperature is not yet increased. These values and evaluated locations shown by arrows are presented in **Fig. 12**, showing that the inflow velocity is gradually decreased from 0.4 m/s at t = 40 ms to 0.08 m/s at t = 300 ms. Thus, the re-attachment of the inner lifted flame, as well as flip-flop between inner and outer flames, could be caused by the reduction of inflow velocity toward the base of the lifted flame, which surely alters the transports of fuel and oxygen. In future, the detailed discussion on the above flame and flow interaction will be conducted, especially focusing on the reaction kernel in the flame base [16].

Fig.11

Fig.12

Conclusions

Focusing on coannular jet flames formed in the triple port burner, the liftoff height and emission

characteristics of soot and NOx were experimentally examined. A numerical simulation was also conducted to discuss the flame structure in detail. Following conclusions were derived.

1. Since two non-premixed flames are formed in the boundaries of fuel and air, there are four flame configurations, consisting of attached flames, inner attached/outer lifted flames, inner lifted/outer attached flames, and twin lifted flames.
2. NOx emission index is decreased only when the outer flame is lifted. On the other hand, the maximum soot concentration in luminous flame is decreased when the inner or outer flame is lifted. These are explained by the fact that fuel and air are partially mixed when the flame is lifted.
3. Based on the flame index, the attached flame is mainly a diffusion flame. When the inner or outer flame is lifted, the so-called triple flame structure is observed. Interestingly, in the case of twin lifted flames, two rich premixed flames are merged each other. By increasing the external air flow velocity, unique flame behaviors are observed, including inner flame re-attachment and flip-flop between inner and outer flames, which could be caused by the reduction of inflow velocity toward the base of the lifted flame.

References

(1) United States Environmental Protection Agency, *Technical Highlights*, EPA420-F03-017, (2003) 1-4.

(2) R. Zhu, M. Guo, F. Ouyang, *Catalysis Today* 139 (2008) 146-151.

(3) N. Peters, S. Donnerhack, *Proc. Combust. Inst*. 18 (1981) 33-42.

(4) T. C. Claypole, and N. Syred, *Proc. Combust. Inst.* 18 (1981) 81-89.

(5) T. Terasaki, and S. Hayashi, *Proc. Combust. Inst*. 26 (1996) 2733-2739.

(6) S. Ishizuka, T. Motodamari, D. Shimokuri, *Proc. Combust. Inst*. 31 (2007) 1085-1092.

(7) J. J. Feese, S. R. Turns, *Combust. Flame* 113 (1998) 66-78.

(8) S. Noda, J. Inohae, and Z. S. Saldi, *Proc. Combust. Inst*. 31 (2007) 1625-1632.

(9) D. Zhao, H. Yamashita, K. Kitagawa, N. Arai, and T. Furuhata, *Combust. Flame* 130 (2002) 352-360.

(10) W. M. Pitts, *Proc. Combust. Inst*. 22 (1988) 809-816.

(11) F. Takahashi, et al., *Proc. Combust. Inst.* 23 (1990) 677-683.

(12) B. J. Lee, J. S. Kim, S. H. Chung, *Proc. Combust. Inst*. 25 (1994) 1175-1181.

(13) M. S. Cha, S. H. Chung, *Proc. Combust. Inst*. 26 (1996) 121-128.

(14) L. Muniz, et al., *Combust. Flame* 111 (1997) 16-31.

(15) T. Fujimori, D. Riechelmann, J. Sato, *Proc. Combust. Inst*. 27 (1998) 1149-1155.

(16) F. Takahashi, et al., *Proc. Combust. Inst.* 28 (2000) 2071-2078.

(17) Y. Mizobuchi, S. Tachibana, J. Shinio, S. Ogawa, T. Takeno, *Proc. Combust. Inst.* 29 (2002) 2009-2015.

(18) Y. Mizobuchi, J. Shinio, S. Ogawa, T. Takeno, *Proc. Combust. Inst.* 30 (2005) 611-619.

(19) H. Tsuji, and I. Yamaoka, *Proc. Combust. Inst.* 19 (1982) 1533-1540.

(20) S. H. Chung, and C. K. Law, *Combust. Flame* 55 (1984) 123-125.

(21) M. Nishioka, T. Takeno, S. Ishizuka, *Combust. Flame* 73 (1988) 287-301.

(22) K. Yamamoto, S. Ishizuka, and T. Hirano, *Proc. Combust. Inst.* 26, (1996), 1129-1135.

(23) H. Oshima, K. Yamamoto, N. Hayashi, H. Yamashita, and G. Okuyama, *Transactions of the Japan Society of Mechanical Engineers*, Series B, 74(748) (2008) 2731-2737.

(24) G. Okuyama, K. Yamamoto, N. Hayashi, and H. Yamashita, *Proc. 6th Int. Conf. Computational Heat and Mass Transfer* (2009) 373-378.

(25) L. G. Blevins, et al., *Proc. Combust. Inst.* 29 (2002) 2325-2333.

(26) L. K. Sze, C. S. Cheung, C. W. Leung, *Combust. Flame* 144 (2006) 237-248.

(27) M. A. Mikofski, et al., *Combust. Flame* 146 (2006) 63-72.

(28) S. S. Yoon, S. M. Lee, S. H. Chung, *Proc. Combust. Inst.* 30 (2005) 1417-1424.

(29) K. Yamamoto, F. Fujikake, Y. Taya, N. Hayashi, H. Yamashita, and S. Gakei, *Transactions of the Japan Society of Mechanical Engineers*, Series B, 74(738) (2008) 224-250.

(30) K. H. Lyle, L. K. Tseng, J. P. Gore, N. M. Laurendeau, *Combust. Flame* 116 (1999) 627-639.

(31) H. Yamashita, G. Kushida, and T. Takeno, *Proc. R. Soc. London*, Ser. A, 431 (1990) 301-314.

(32) H. Yamashita, M. Shimada, and T. Takeno, *Proc. Combust. Inst.* 26 (1996) 1226-1233.

(33) M. D. Smooke, *Reduced Kinetic Mechanisms and Asymptotic Approximations for Methane-Air Flames*, Springer-Verlag, Berlin, Germany, 1991.

Figure captions

Fig. 1 Schematic of the triple port burner.

Fig. 2 Analytical model and coordinate system.

Fig. 3 Photographs of flames in the triple port burner. Four flame configurations of (a) attached flames, (b) inner attached/outer lifted flames, (c) inner lifted/outer attached flames, (d) twin lifted flames are observed.

Fig. 4 Phase diagram of flames.

Fig. 5 Variations of liftoff height with external air flow velocity at (a) $U_{1A} = 0.4$ m/s, (b) $U_{1A} = 0.6$ m/s, (c) $U_{1A} = 0.8$ m/s; $U_{2F} = 0.6$ m/s.

Fig. 6 Variations of maximum LII signal with external air flow velocity at (a) $U_{1A} = 0.4$ m/s, (b) $U_{1A} = 0.6$ m/s, (c) $U_{1A} = 0.8$ m/s; $U_{2F} = 0.6$ m/s.

Fig. 7 Variations of NOx emission index with external air flow velocity at (a) $U_{1A} = 0.4$ m/s, (b) $U_{1A} = 0.6$ m/s, (c) $U_{1A} = 0.8$ m/s; $U_{2F} = 0.6$ m/s.

Fig. 8 Distributions of temperature, mass fractions of fuel and oxygen, and heat release rate; $U_{1A} = 0.7$ m/s, $U_{2F} = 0.6$ m/s; $U_{3A} = 0.1$ m/s.

Fig. 9 Distributions of heat release rate at (a) $U_{3A} = 0.1$ m/s, (b) $U_{3A} = 0.4$ m/s, (c) $U_{3A} = 0.8$ m/s, (d) $U_{3A} = 1.1$ m/s; $U_{1A} = 0.7$ m/s, $U_{2F} = 0.6$ m/s.

Fig. 10 Distributions of flame index at (a) $U_{3A} = 0.1$ m/s, (b) $U_{3A} = 0.4$ m/s, (c) $U_{3A} = 0.8$ m/s, (d) $U_{3A} = 1.1$ m/s; $U_{1A} = 0.7$ m/s, $U_{2F} = 0.6$ m/s.

Fig. 11 Distributions of temperature by changing external air flow velocity from 1.0 to 1.1 m/s at (a) $t = 40$ ms, (b) $t = 120$ ms, (c) $t = 240$ ms, (d) $t = 300$ ms, (e) $t = 400$ ms; $U_{1A} = 0.7$ m/s, $U_{2F} = 0.6$ m/s. Temperatures of inner and outer flames at leading flame edge are shown.

Fig. 12 Distributions of heat release rate by changing external air flow velocity from 1.0 to 1.1 m/s at (a) $t = 40$ ms, (b) $t = 120$ ms, (c) $t = 240$ ms, (d) $t = 300$ ms, (e) $t = 400$ ms; $U_{1A} = 0.7$ m/s, $U_{2F} = 0.6$ m/s.

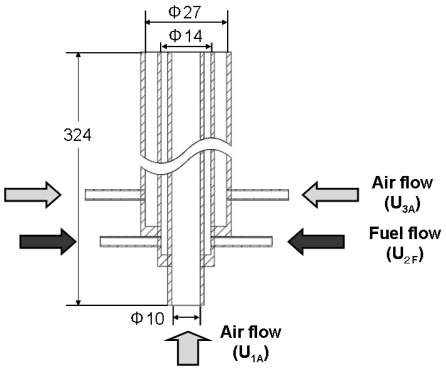

Fig. 1 Schematic of the triple port burner.

[Word Count] = (50+10)*2.2*1 + 8 (caption) = 140 words

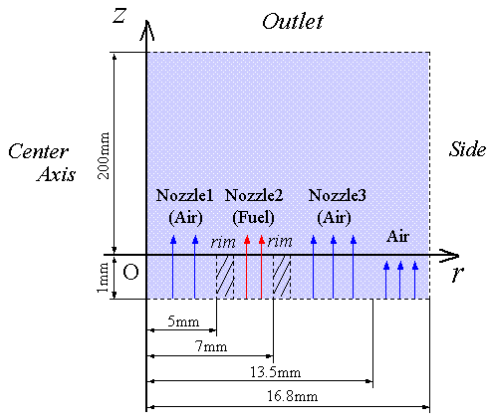

Fig.2 Analytical model and coordinate system.

[Word Count] = (55+10)*2.2*1 + 6 (caption) = 149 words

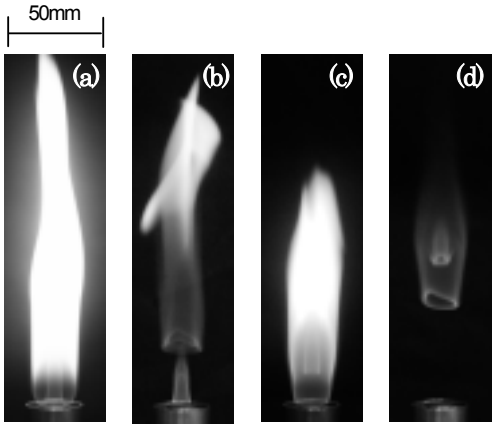

Fig. 3 Photographs of flames in the triple port burner. Four flame configurations of (a) attached flames, (b) inner attached/outer lifted flames, (c) inner lifted/outer attached flames, (d) twin lifted flames are observed.

[Word Count] = (55+10)*2.2*1 + 33 (caption) = 176 words

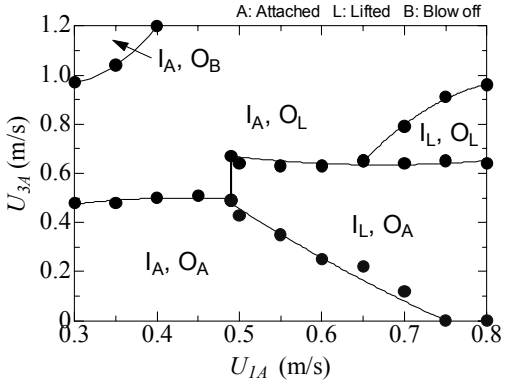

Fig. 4 Phase diagram of flames.

[Word Count] = (50+10)*2.2*1 + 6 (caption) = 138 words

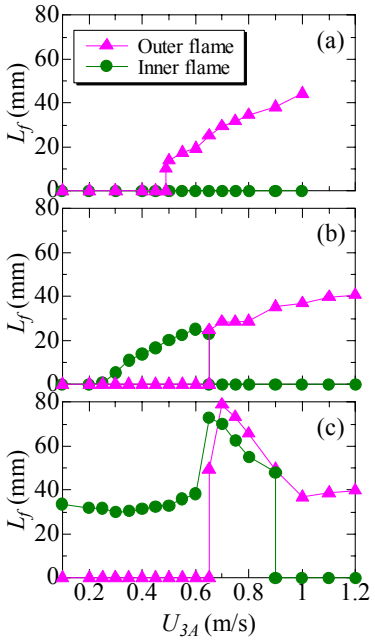

Fig. 5 Variations of liftoff height with external air flow velocity at (a) U_{1A} = 0.4 m/s, (b) U_{1A} = 0.6 m/s, (c) U_{1A} = 0.8 m/s; U_{2F} = 0.6 m/s.

[Word Count] = (85+10)*2.2*1 + 32 (caption) = 241 words

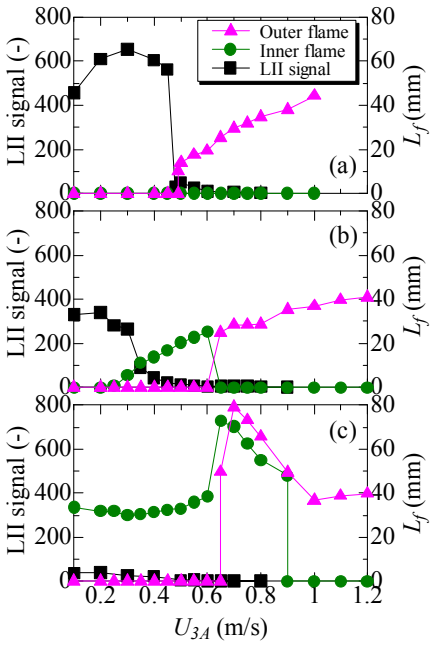

Fig. 6 Variations of maximum LII signal with external air flow velocity at (a) U_{1A} = 0.4 m/s, (b) U_{1A} = 0.6 m/s, (c) U_{1A} = 0.8 m/s; U_{2F} = 0.6 m/s.

[Word Count] = (85+10)*2.2*1 + 32 (caption) = 241 words

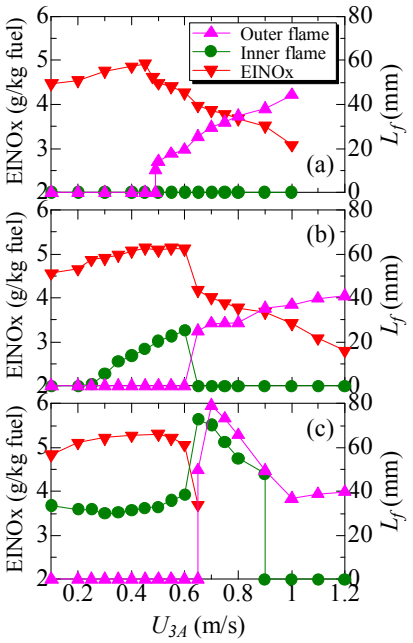

Fig. 7 Variations of NOx emission index with external air flow velocity at (a) U_{1A} = 0.4 m/s, (b) U_{1A} = 0.6 m/s, (c) U_{1A} = 0.8 m/s; U_{2F} = 0.6 m/s.

[Word Count] = (85+10)*2.2*1 + 32 (caption) = 241 words

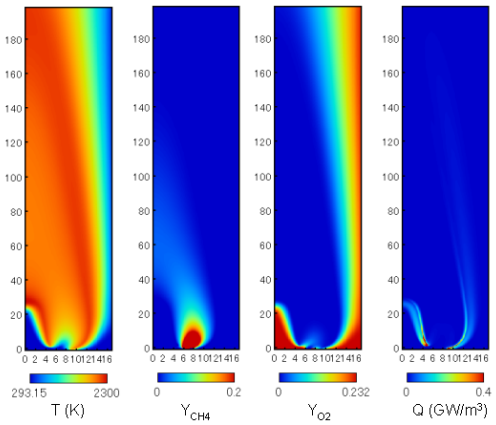

Fig. 8 Distributions of temperature, mass fractions of fuel and oxygen, and heat release rate; U_{1A} = 0.7 m/s, U_{2F} = 0.6 m/s; U_{3A} = 0.1 m/s.

[Word Count] = (55+10)*2.2*1 + 27 (caption) = 170 words

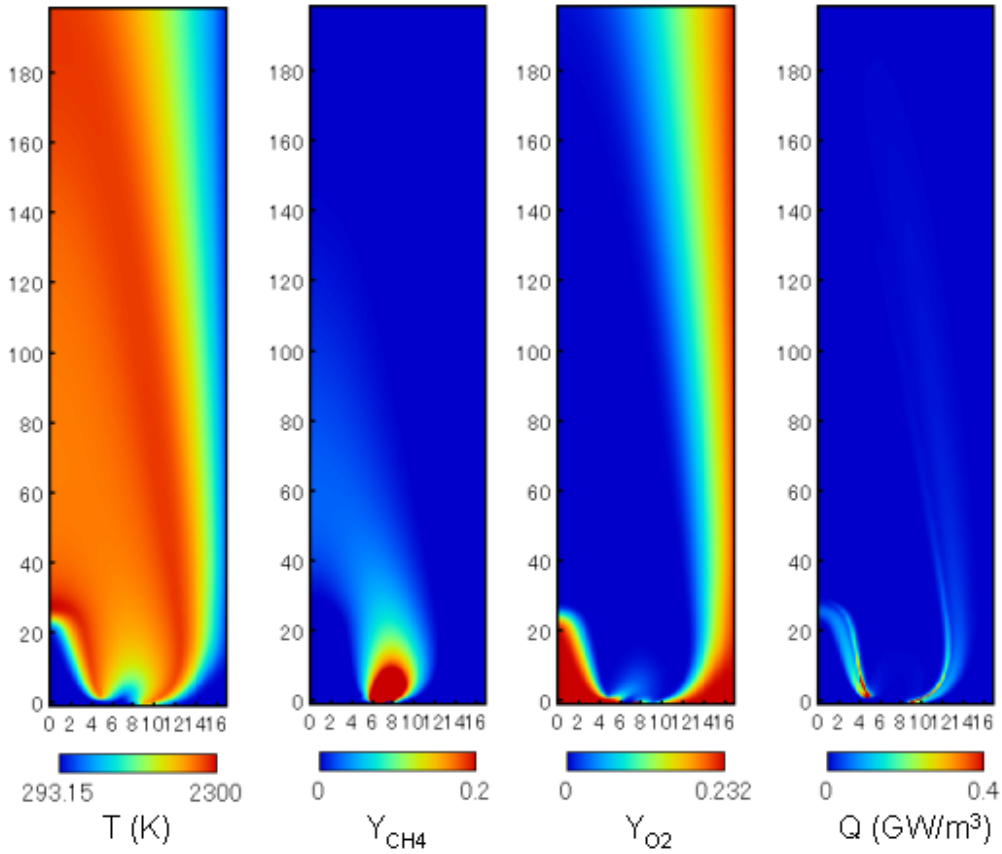

Fig. 8 (enlarged)

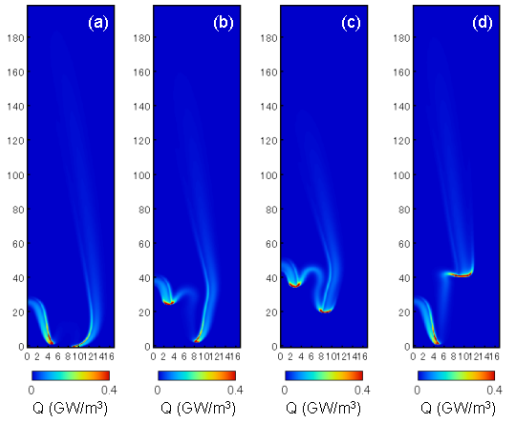

Fig. 9 Distributions of heat release rate at (a) U_{3A} = 0.1 m/s, (b) U_{3A} = 0.4 m/s, (c) U_{3A} = 0.8 m/s, (d) U_{3A} = 1.1 m/s; U_{1A} = 0.7 m/s, U_{2F} = 0.6 m/s.

[Word Count] = (55+10)*2.2*1 + 36 (caption) = 179 words

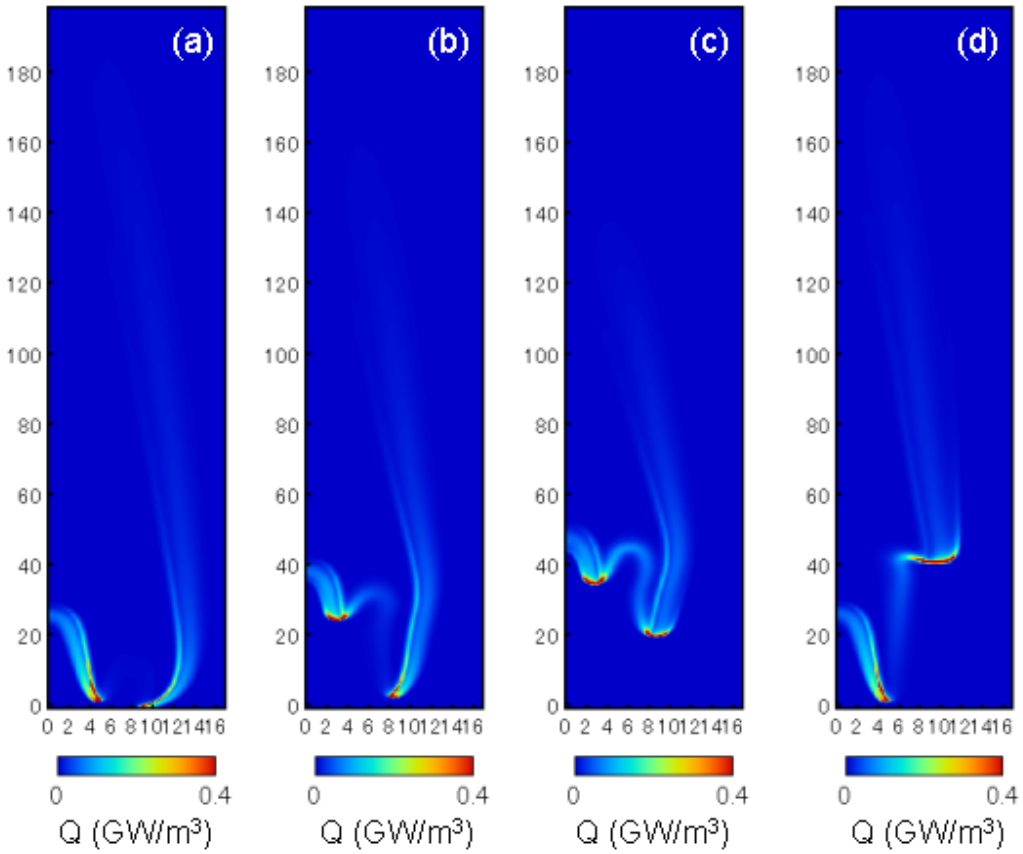

Fig. 9 (enlarged)

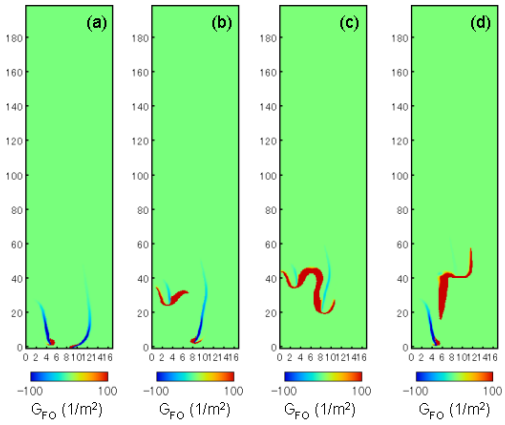

Fig. 10 Distributions of flame index at (a) U_{3A} = 0.1 m/s, (b) U_{3A} = 0.4 m/s, (c) U_{3A} = 0.8 m/s, (d) U_{3A} = 1.1 m/s; U_{1A} = 0.7 m/s, U_{2F} = 0.6 m/s.

[Word Count] = (55+10)*2.2*1 + 35 (caption) = 178 words

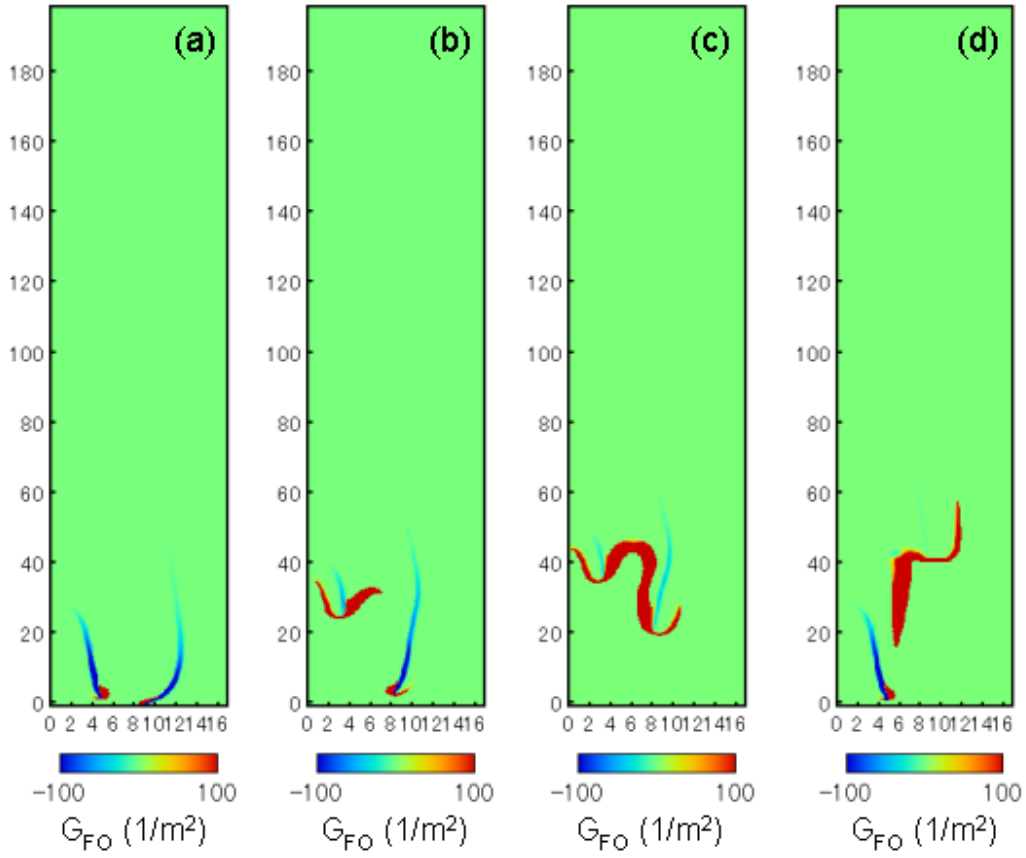

Fig. 10 (enlarged)

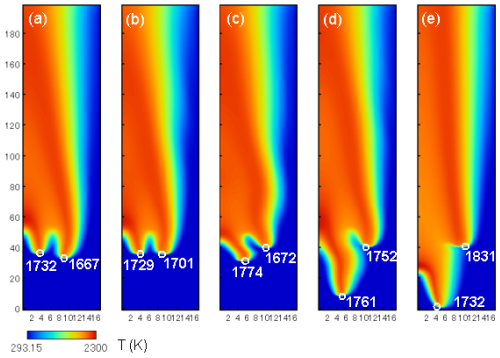

Fig. 11 Distributions of temperature by changing external air flow velocity from 1.0 to 1.1 m/s at (a) t = 40 ms, (b) t = 120 ms, (c) t = 240 ms, (d) t = 300 ms, (e) t = 400 ms; U_{1A} = 0.7 m/s, U_{2F} = 0.6 m/s. Temperatures of inner and outer flames at leading flame edge are shown.

[Word Count] = (50+10)*2.2*1 + 62 (caption) = 216 words

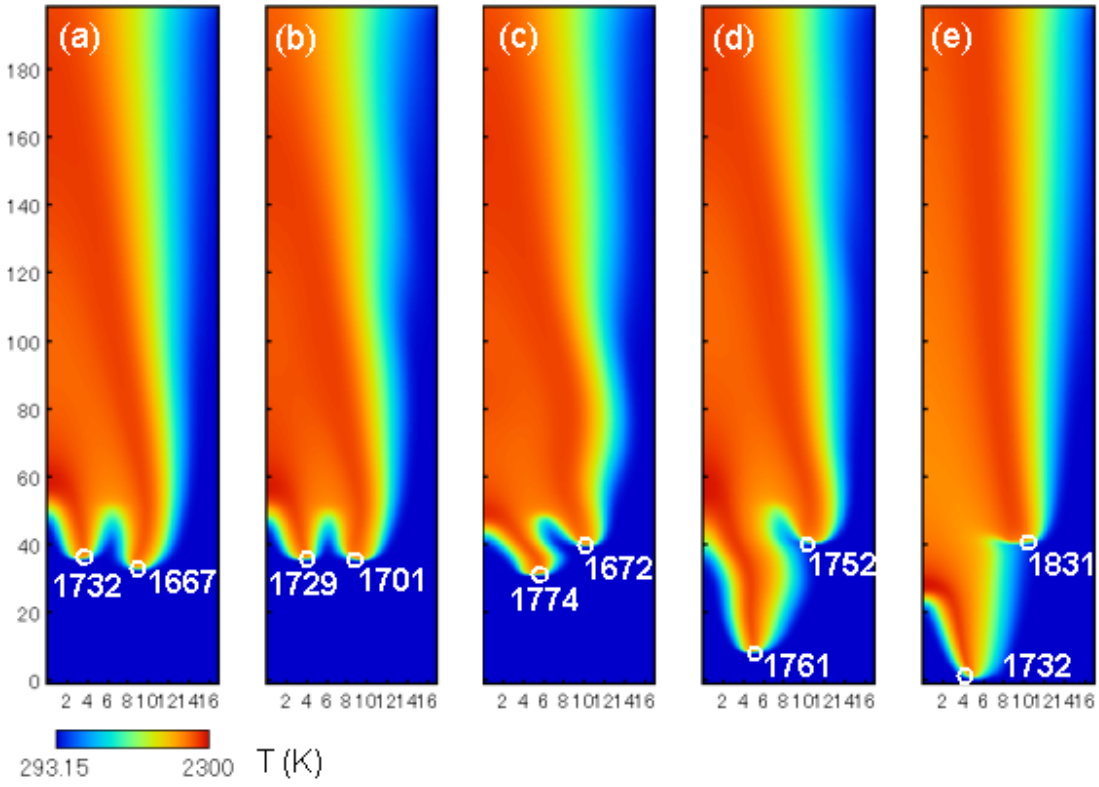

Fig. 11 (enlarged)

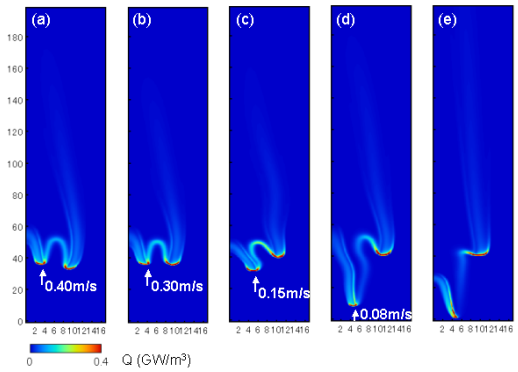

Fig. 12 Distributions of heat release rate by changing external air flow velocity from 1.0 to 1.1 m/s at (a) t = 40 ms, (b) t = 120 ms, (c) t = 240 ms, (d) t = 300 ms, (e) t = 400 ms; U_{1A} = 0.7 m/s, U_{2F} = 0.6 m/s.

[Word Count] = (50+10)*2.2*1 + 52 (caption) = 184 words

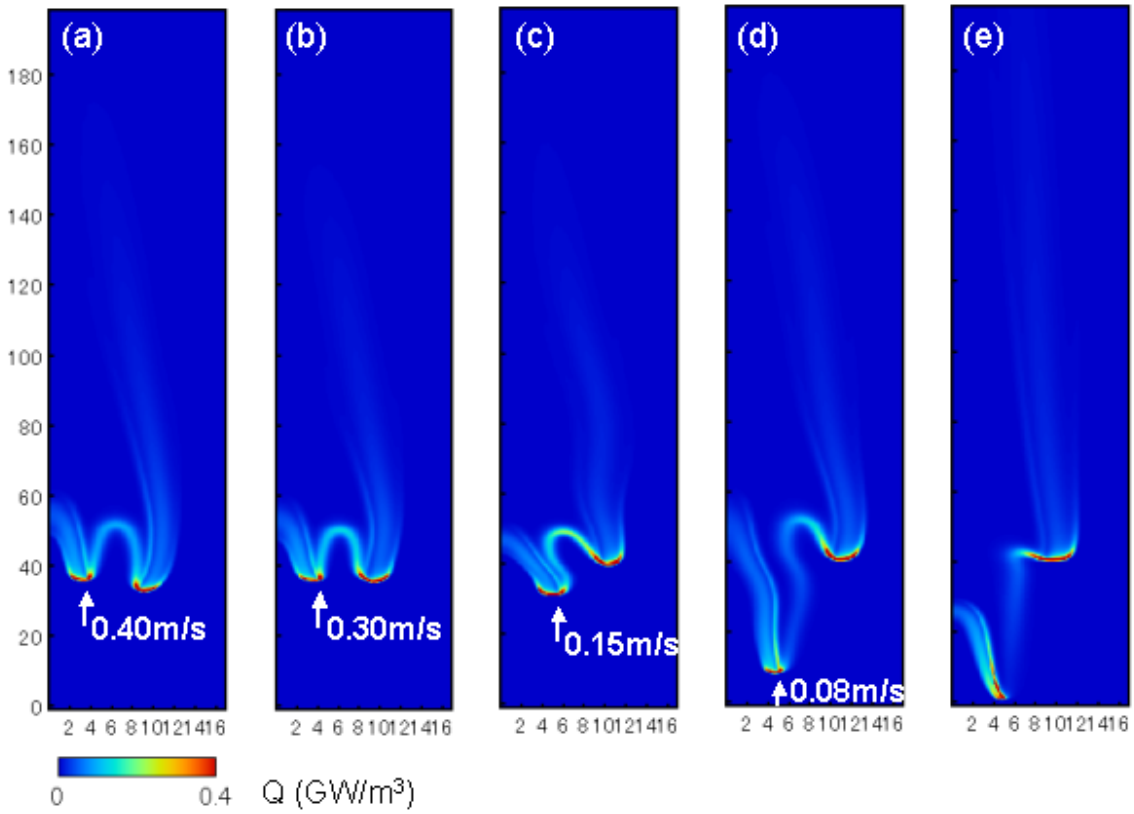

Fig. 12 (enlarged)